Charge state distributions of scattered and recoil ions in C^+–, F^+–, and Ne^+–Si-surface collisions

B. Hird, R. A. Armstrong, and P. Gauthier
Ottawa-Carleton Institute for Physics, Ottawa University Campus, Ottawa, Ontario, Canada KIN 6N5
(Received 15 June 1993)

The proportions of keV ions, incident on a clean silicon surface, which are scattered as doubly or triply charged ions are found to increase with atomic number from C^+ to Ne^+. In contrast, the recoil Si^{2+} and Si^{3+} ion yields decrease. A definite collision-energy threshold for the production of each of these multicharged ions is found. All the multicharged recoil silicon ion thresholds are consistent with inner-shell vacancy production at the $3d\sigma$-$3p\pi$ level crossing. However, the multicharged scattered ions seem to be produced by a different process. The surface-scattered ion yields may follow the same systematics as x-ray yields, which pass through maxima when the shell energies match.

PACS number(s): 79.20.Rf, 34.70.+e

I. INTRODUCTION

When ions of a few keV kinetic energy strike a solid surface, it has been established [1,2] that considerable proportions of both the ingoing ions which have been scattered back out from the surface, and also the recoiling target atoms, are multicharged.

These multicharged ions must be distinguished from the low energy ions which have long been known from secondary-ion mass spectrometry (SIMS) measurements [3]. Wittmaack [4] showed that the yield of low-energy Si^{2+} ions was closely proportional to the *LMM* Auger-electron yields over several orders of magnitude as the energy of the noble-gas incident ions was varied from threshold to 30 keV, providing strong evidence that the multicharged ions and the Auger electrons are the result of the same ion-solid interaction processes.

Wittmaack also found that the yields of Si^{2+}, produced by bombardment with Ne^+, Ar^+, Kr^+, and Xe^+ were very similar to each other when plotted as functions of the maximum energy transferred in a head-on collision. He proposed that this was evidence that the inner-shell vacancies were produced in symmetric collisions, when recoiling target atoms make hard collisions with other target atoms (t-t collisions), rather than in asymmetric projectile-target (p-t) collisions. Considerable work has since been done to establish the relative importance of t-t compared to p-t collisions [5–8] in the Auger-electron yields. For a recent review see Valeri [9]. A weak line in the Auger spectrum has been attributed to the decay from double vacancy excitations, and the incident ion energy threshold to produce this line was found to be considerably higher than for the other Auger transitions. Such double vacancies are probably necessary for the production of multicharged ions. However, it is only in p-t collisions that both vacancies are likely to be produced in a single partner since symmetric collisions strongly favor one vacancy in each partner. Asymmetric p-t collisions may thus be the main source of multicharged ions, even though symmetric t-t collisions are the main source of Auger electrons.

Deductions about the collision processes which create multicharged ions are very indirect from both SIMS and Auger-electron measurements. SIMS measures low-energy ions which have made many collisions before they are detected by the quadrupole mass spectrometer. Auger electrons are emitted approximately isotropically in the moving frame of the ion or atom which emits them, so that its direction is unknown apart from a small Doppler shift, so that only a statistical average is obtained.

In the measurements reported here the collision trajectories are well defined. We select peaks in the energy spectrum of the emitted ions which agree well with the energies predicted from single binary encounters, where either the incident ion or the recoil atom is scattered directly out of the surface without further loss of energy. Both correspond to the asymmetric p-t process.

In contrast to the situation at higher energies [10], the average charge of the emitted ions from binary collisions is found to be less than in corresponding ion-gas collisions. We previously reported the observation of doubly and triply charged ions from N^+-Si and O^+-Si collisions in measurements which selected single ion scattering events with the top surface layer atoms. Here we report an extension of these measurements using beams of C^+, F^+, and Ne^+ ions to investigate the dependence of multicharged ion production on Z_1, the projectile atomic number.

A definite kinetic energy threshold was found for the appearance of each multicharged ion species. This is consistent with a model which restricts the production process to a well defined ion-atom separation, which is just reached by ions of threshold kinetic energy at the distance of closest approach, during the ion-atom collision. We previously found that all the N^+-Si and O^+-Si interaction distances were the same (about 0.2 Å), within the accuracy of the measurements. These interaction distances are much smaller than the nearest-neighbor sep-

arations of the atoms in the solid (3.8 Å), so that the multicharged ion creation process should be substantially independent of the properties of the solid. However, these multicharged ions, once formed at a close encounter, may be partly neutralized by subsequent soft interactions with other atoms before they escape from the surface. The interaction distance is in rough agreement with an estimate of the region in the correlation diagram where the $3d\sigma$ molecular orbital crosses the $3p\pi$ orbital. In the electron promotion model [11] electron transitions mainly occur at these crossings, and result in the transfer of electrons from the $2p$ shell of Si into the partly filled $3p$ shell, so that the production of Si^{2+} and Si^{3+} ions can be understood in terms of the emission of two or three electrons, as the L-shell vacancies in the recoiling silicon atoms are filled by Auger transitions. However, electron promotion at the $3d\sigma$-$3p\pi$ crossing can only result in the production of N^{2+} or O^{2+} ions if there is some transfer of ionization or vacancy sharing before the molecular states separate into two distinct atoms.

There is considerable information on the conditions under which vacancies in atomic shells are produced [12]. The vacancies may be detected experimentally by the x rays, or the Auger electrons which are emitted, as the vacancies are filled. Large systematic variations with the beam and with the target atomic numbers, Z_1 and Z_2, respectively, have been found in ion-gas collisions. X-ray production [13] shows a strong correlation with shell binding energies, with a maximum when the binding energy in the target matches that in the projectile. This has also been observed very clearly in solids where Kavanagh *et al.* [14] found very large oscillations [(peak)/(valley) >100] in the yield of Cu x rays when keV ions bombarded a copper target, and also when Cu^+ ions bombarded a variety of solid targets, with maxima where there was a binding energy match between the copper L-shell and either the L-shell or the K-shell energy of the beam particles. They also found that most of the x rays came from the lower Z atom when $Z_1 \approx Z_2$. The shell matching was discussed by Barat and Lichten [11] within the framework of the electron promotion model.

The matching energy of shell binding energies may also account for the oscillations found by Lennard and Phillips [15] in the mean charge on MeV ions which had reached charge equilibrium after passing through carbon foils a few hundred atomic layers thick. The mean charge peaked for beam ions with $Z_1 = 16$ or 17. Allowing for some depression of the L-shell energy due to the ionized state of the projectile, there is a match with the K-shell energy of carbon. In contrast, similar measurements with Al targets [16], where there is no K-shell match, showed no similar maximum.

II. EXPERIMENT

The ions from the source were accelerated, momentum selected, and then passed through a differential section into the 1.5×10^{-10} Torr vacuum environment of the target. The scattered ions were energy analyzed with a $\pi/\sqrt{2}$ deflection electrostatic analyzer (ESA) mounted on a racetrack inside the target chamber, and counted with a channel electron multiplier (CEM) at its image plane [2]. Scattering angles were chosen such that the surface-scattered single collision peaks were resolved from each other, and to minimize the proportions of subsurface and multiply scattered ions.

The ions were produced in a rf-discharge source which was run on CO gas for the C^+ beam, and on CF_4 (freon 14) gas for the F^+ beam. The accelerator, which had been designed for ~100-keV operation, was modified for lower energies. Adequate ion currents were maintained down to a few keV by placing a large negative voltage halfway down the accelerator column. The accelerated ions were momentum selected by a 30° deflection magnet, and then passed through a differentially pumped section defined by 2-mm- and 0.3-mm-wide apertures which were separated by a distance of 120 cm. This section both isolated the vacuum of the scattering chamber from the accelerator and defined the ion beam profile at the target just beyond the second aperture. With a pressure of 8×10^{-9} Torr in the differential section there was no detectable pressure difference in the target region due to either the gas flow or the ion beam from the accelerator.

The ion source produced a less intense F^+ beam than was obtained for the other ions. It was found that there was considerable loss of ions through the very tight geometry of the apertures which defined the differential section. The 1-nA beam which was previously used was close to the theoretical limit set by the space charge repulsion between the ions in this region [17]. To compensate for this space charge increase in the beam size, an einzel lens was placed halfway between the apertures to refocus the ions. The proportion of the ions reaching the target was thereby increased considerably.

As a measure of beam intensity, for normalizing the ESA counts, it was found unreliable to use the measured beam current on the target, probably due to variations in the secondary emission from the target to the surroundings, and to short time variations of the very small current, which could not be followed by a picoammeter. To avoid both problems, the ESA count at each voltage step in the scan was scaled to the counts from a second CEM placed behind a 15-μm-diam aperture 12 cm from the target, where it could count all the ions scattered at a fixed backward angle.

An amorphous surface was chosen so as to avoid the anisotropies produced by shadowing and blocking effects in a single crystal. These are known to influence the emitted ion charge states [1,18]. During ion bombardment, surface damage might change the surface structure of a single crystal, and so change the scattered and recoil ion yield in certain directions. The target was a wafer of Si(100) which had been sputter cleaned with 500-eV Ar^+ ions. Each sputter cleaning was followed by a partial anneal to approximately 500 °C for about 10 sec. After this time most of the argon implanted during the sputtering was desorbed, as indicated by the return of the pressure, and the residual gas composition, to its value before heating. This heating was not sufficient to anneal the surface back to a single crystal [19]. Reflection high-energy-electron diffraction (RHEED) measurements

showed no diffraction spots, whereas the same target annealed to 900 °C for 20 min produced the sharp (2 × 1) pattern expected from the surface reconstruction. To test the amorphous condition of the target, the variation of scattered peak intensities was determined as the target was rotated in its own plane. An angle of incidence to the surface of 5° was chosen, as being well inside the shadow cone angle of adjacent surface atoms. No statistically significant variation was found. Repeating this measurement with the fully annealed Si(100) single-crystal surface showed the expected decrease in intensity along the ⟨110⟩ direction.

Carbon is considered one of the more difficult elements to remove from a silicon surface, and is often a serious contaminant. However, it has been reported that islands of SiC can be removed by sputtering though not by heating [20]. Special care was taken that such contamination did not affect the data. Each scan of the energy spectrum took about 3 min, compared to about 2 h for the beam to strike every surface atom, so that by sputter cleaning the surface after every few measurements the carbon buildup on the surface was negligible. The measurements showed no indication of a peak in the energy spectrum where C^+-C scattering would be observed. To determine the effect on the data of surface contamination by carbon, tests were made without sputter cleaning between measurements. The main change was found to be a decrease in the scattered ion peak areas, with a smaller decrease in the recoil ion peaks, and a slight increase in the background. The different charge states were affected about equally, so that inadequate sputter cleaning would not significantly change the ratio of the peak areas shown in Fig. 2. A similar reduction in peak intensity was not found in the previous measurements with N^+ and O^+ ion beams.

III. RESULTS

Figure 1 shows electrostatic analyzer voltage scans of the ions from the surface which are emitted at 45° to the incident beam direction. The peaks can all be identified as scattered, or recoil ions from single collision events in the top atomic layers. The peak positions agree well with the energies predicted from elastic scattering kinematics. Doubly charged and triply charged ions require, respectively, half and one-third of the deflection voltage of singly charged ions of the same energy, and the deflection voltages for the assigned multicharged ion peaks were always found to be in these ratios to an accuracy of one channel. As a verification that these were indeed multicharged ions, measurements were repeated over a range of scattering angles. Throughout, the ratio was found to be constant, whereas it would have changed if we were observing recoiling singly charged ions from heavy atom surface impurities.

Ions which have made two or more small angle collisions with surface atoms have more energy than those where the same total deflection is produced in a single collision. Such events appear as shoulders on the high-energy side of the peaks. The proportion of these multiply scattered ions is found to increase with Z_1, and is most evident for Ne^+. To exclude multiple scattering and estimate the yield of ions which had made single collisions, a Gaussian distribution of adjustable width, position, and height was subtracted from the peak region, until a monotonic background underneath was obtained.

Figure 2 shows the relative yields of the ions which have made single atomic collisions as a function of the beam atomic number Z_1. Figure 2(a) shows the scattered ion yields, and Fig. 2(b) the recoiling silicon ion yields. For comparison these were all measured at the same collision velocity of 0.526 keV/amu. In calculating the yields, the areas under the peaks in the voltage scans were corrected for the variation of the ESA resolution with ion energy and with charge state.

There are large differences in the ion yields between $Z_1 = 6$ and $Z_1 = 10$. With the carbon beam, the yields from the surface consist almost completely of recoiling silicon ions, whereas with the neon beam we could detect only a small number of recoil ions, but there was a large yield of scattered ions. The differences cannot be associated with the ionization potentials, which increase

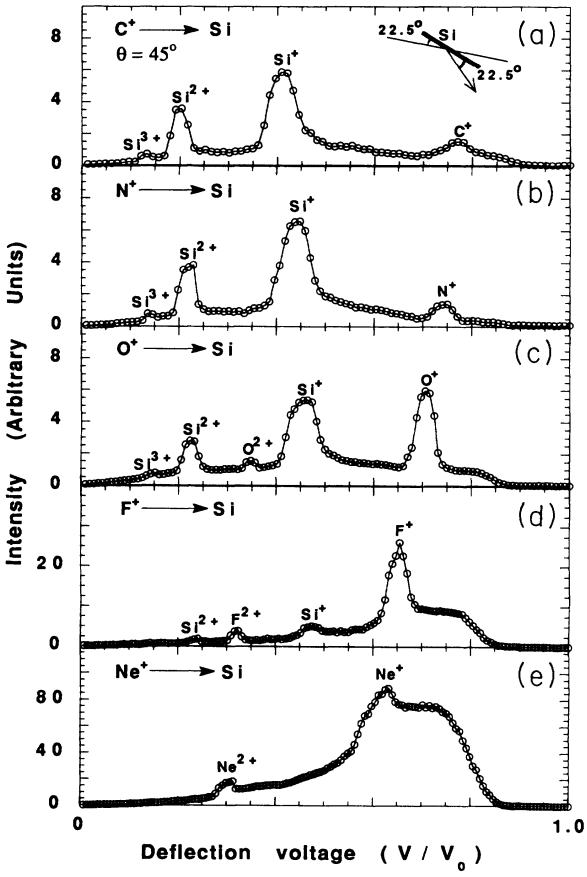

FIG. 1. Electrostatic analyzer (ESA) spectrum of ions emitted at $\theta = 45°$ to the incident ion direction from a clean silicon amorphous surface. V is the deflection voltage, and V_0 is the voltage required to deflect the direct incident ion beam through the ESA. The same incident ion velocity 0.526 keV/amu was used for all the measurements. The incident beams were (a) C^+; (b) N^+; (c) O^+; (d) F^+, and (e) Ne^+.

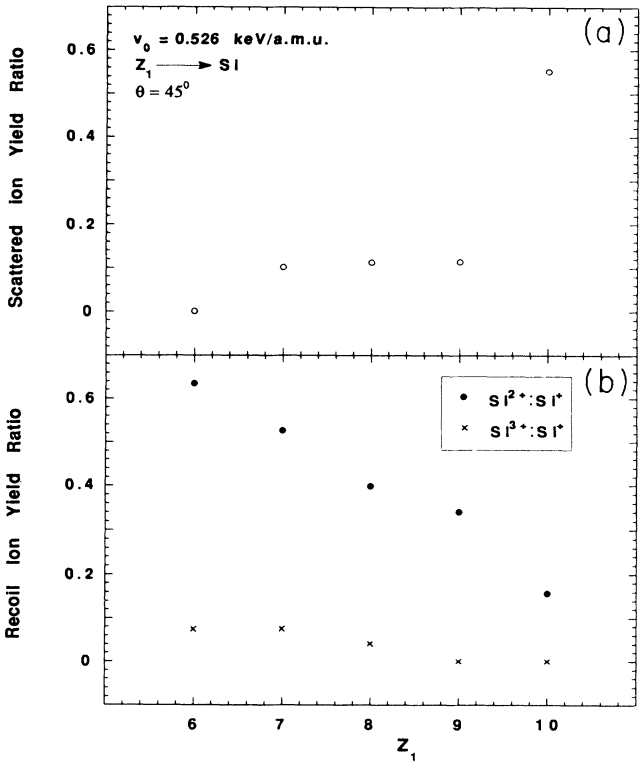

FIG. 2. Relative yields of doubly and triply charged to singly charged ions, as a function of incident beam atomic number Z_1. Open circles are for doubly charged to singly charged scattered ion ratios. Solid circles are for Si^{2+}:Si^+, and crosses are for Si^{3+}:Si^+. (a) Scattered ions. (b) Recoil silicon ions.

from 11.2 eV in carbon to 21.5 eV in neon, so that loss of scattered ions to neutralization should be largest for the Ne^+ beam [21]. Not only are there more singly scattered ions with this beam, but relative to these there are more multiply scattered neon ions. The scattering cross section, in any of the forms which is used to fit ion-atom collisions, increases continuously with Z_1, so that clearly some other interaction process than potential scattering is responsible for the opposite behavior of the scattered and recoil ion yields.

A definite energy threshold was observed for the presence of multicharged ions. In all cases, as the beam energy was decreased, the ESA spectra simplified to only singly charged ion peaks and a continuous background from subsurface scattering. The thresholds listed in Table I are the lowest beam energies at which the multicharged ion peak could be identified above the background.

The existence of thresholds is consistent with interactions, which occur only at definite interatomic separations. We have made exact calculations of the ion-atom trajectories using the "universal" potential which O'Connor and Biersack [22] found as the best fit to a wide range of scattering interactions. No adjustable parameters were used with this potential, but we found that it produced effectively identical shadow cone predictions to the Ziegler-Biersack-Littmark potential [23] in which the screening length was used as an adjustable parameter so as to fit experimentally determined shadow cones [24]. Table I also lists the distances of closest approach (r_0), calculated using this potential at the measured threshold energies and scattering angles. These values are shown in Fig. 3, where they are plotted as a function of Z_1, the beam atomic number.

Interpretation of electron vacancy production during ion-atom collisions is usually done in terms of the molecular orbital model. As the separation between the two particles decreases, the atomic electron states rearrange to fill molecular orbitals, subject to the Pauli principle. The relative energies of these states change with ion-atom separation, and electron transfer is thought to mainly occur when molecular orbital states mix at near degeneracies. After the collision, the electrons may not return to their initial orbitals, and vacancies in lower-energy orbitals are produced. A characteristic of the electron promotion model is that the near degeneracy usually occurs at a definite particle separation which is called the crossing radius. If the trajectory does not bring the two particles close enough together to reach the crossing radius during the collision, then no vacancies are produced.

A. Si^{2+} and Si^{3+} recoil ions

Figure 2(b) shows that the production of Si^{2+} and Si^{3+} recoil ions in surface collisions decreases continu-

TABLE I. Energy thresholds E_t, and distances of closest approach r_0, calculated with the "universal" screened Coulomb potential of O'Connor and Biersack [22]. θ is the angle between the incident ion direction and the detected ion direction. θ' is the scattering angle when recoil Si ions are detected at θ.

Beam	θ	θ'	Doubly charged		Triply charged		Si^{2+}		Si^{3+}	
			E_t (keV)	r_0 (Å)	E_t (keV)	r_0 (Å)	E_t (keV)	r_0 (Å)	E_t (keV)	r_0 (Å)
C^+	40°	75°	12.5[a]	0.128			2.6	0.241	3.1	0.221
N^+	40°	72°	7.3	0.187			3.8	0.217	5.3	0.181
O^+	40°	68°	5.8	0.228	15.0[b]	0.114	5.5	0.195	8.3	0.154
F^+	40°	63°	3.8	0.300	12.3	0.159	7.4	0.181	12.0	0.136
Ne^+	50°	48°	0.8	0.558	11.1	0.164	9.8	0.179	17.0[c]	0.123

[a] $\theta = 36°$.
[b] $\theta = 55°$.
[c] $\theta = 45°$, $\theta' = 54°$.

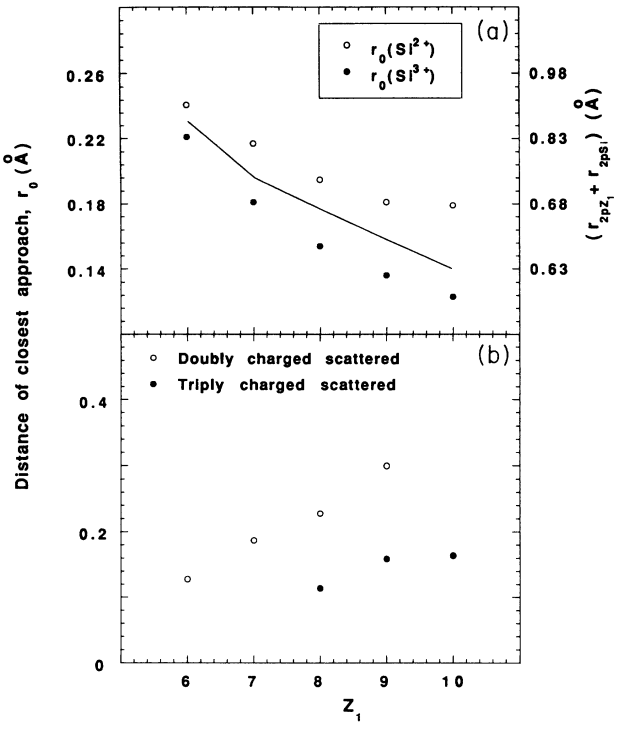

FIG. 3. Distance of closest approach during single ion-atom collisions, calculated using a "universal" screened Coulomb potential [22]. Open circles are for doubly charged ions, and solid circles are for triply charged ions. (a) Silicon recoil ions; (b) Scattered incident ions. The line connects values of the sum of the atomic radii of the projectile and the target, calculated from the maximum of the Hartree-Fock electron densities [28].

ously from C^+ to Ne^+, and is accompanied by a corresponding decrease in the crossing radius (Fig. 3). In N^+-Si and O^+-Si collisions, these interaction distances were identified with a crossing radius at which one or two of the six $2p$ shell electrons from Si which occupy the $3d\sigma$ orbital of the temporary molecule are transferred to the $3p\pi$ orbital, so that these electrons are promoted to the $3p$ shell of Si when the atoms separate [2]. Figure 4 shows correlation diagrams where the molecular states, at finite atomic separation, diabatically connect the separated-atom energy levels to the combined-atom levels having the same quantum numbers and symmetries. The rules for drawing these diagrams are given by Barat and Lichten [11]. The diagrams are shown for C-Si and Ne-Si, and it can be seen that though there are differences in the level spacing the level order is almost the same, and the same $3d\sigma$ to $3p\pi$ crossing is therefore likely to be responsible for electron promotion with all projectiles from C^+ to Ne^+. A crude estimate of the crossing radius was obtained by scaling the crossing radius in Ne^+-Ar where the correlation diagram energies have been calculated [25]. These have a quite similar $Z_1 : Z_2$ ratio to N^+-Si and O^+-Si, and the level ordering is the same. It was estimated that the interaction radius should scale as $(Z_1 Z_2)^{-1}$, so that the 0.112 Å value in Ne^+-Ar would become 0.206 Å in N^+-Si, and 0.180 Å in O^+-Si, in rough agreement with both the scattered and recoil ion distances of closest approach.

If the same $3d\sigma$ - $3p\pi$ crossing is also responsible for Si^{2+} and Si^{3+} ion production in C^+-Si, F^+-Si, and Ne^+-Si, then a decrease in r_0 with Z_1 is expected as the inner-shell electrons become more tightly bound by the higher nuclear charge. The $(Z_1 Z_2)^{-1}$ scaling factor cannot be

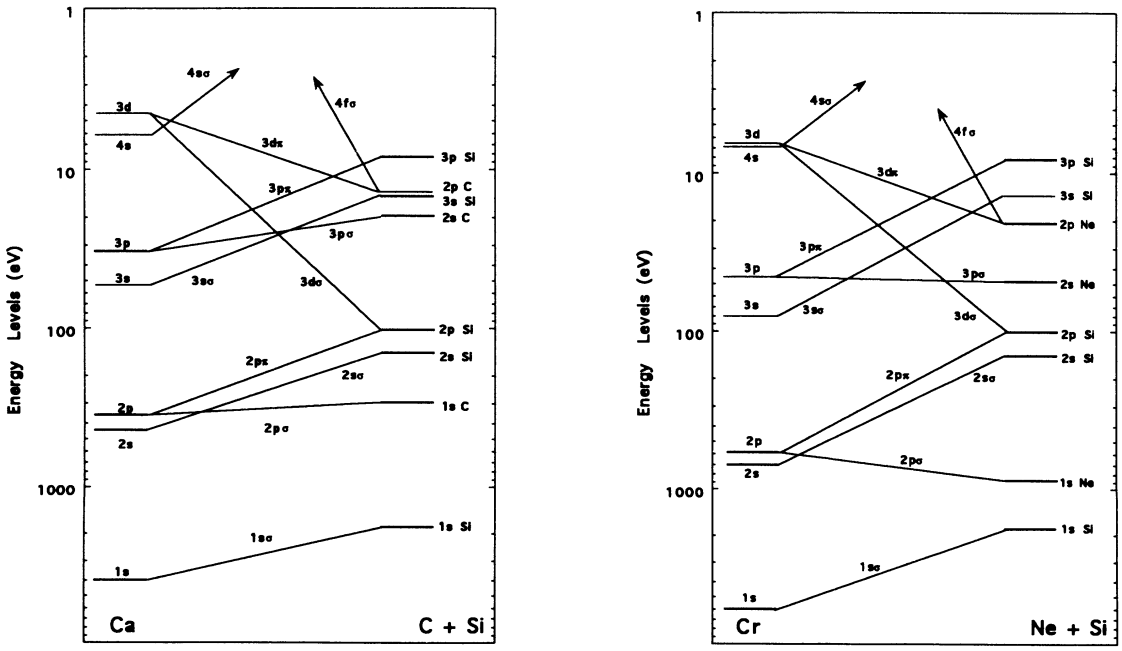

FIG. 4. C-Si and Ne-Si correlation diagrams. The diabatic notation [11] is used to label the molecular orbitals which, in this approximation, connect the atomic states at infinite separation to the united atom states.

used here to estimate the Z_1 dependence, since this scaling assumes a constant $Z_1 : Z_2$ ratio. However, Fastrup *et al.* [26] made energy loss measurements in ion–Ar-gas collisions using several ion beams, and compared their experimental r_0 values, which are associated with the promotion of one electron from the $2p$ shell [27], with the sum of the target and projectile $2p$ shell atomic radii. Though their experimental r_0 values were always smaller than this sum, they showed the same Z_1 dependence.

The sum of the $2p$ shell radii, as given by Hartree-Fock calculations for the maxima in the electron density [28], are shown as a line in Fig. 3. There is rough agreement in the variation with Z_1 for both Si^{2+} and Si^{3+}, confirming that the recoil ions in all these ion-Si collisions are probably the result of the same level crossing. The values are everywhere too large by a factor of about 3, showing that there is considerable overlap of the wave functions, which are far from being atomic orbitals at these small nuclear separations. However, the variation with Z_1 should be roughly valid.

The Si^{3+} crossing radii are always less than the corresponding Si^{2+} radii. A systematic difference is expected because of the increase in binding energy with the number of holes in the L shell. Si^{3+} ions require more Auger transitions to further ionize the silicon recoil atom than do Si^{2+} ions, so it is likely that there is a correlation between the number of $2p$ shell holes which are produced in a collision, and the final recoil ion charge state which results. Larkins [29] has calculated the shell energies for Ar states having one or two L-shell vacancies. He found that the double hole states have binding energies about 15% greater than the equivalent single hole states. Such an increase in the binding energies could account for the observed decrease in the crossing radii.

B. Scattered multicharged ions

The scattered ion yields have a strikingly different Z_1 dependence from the Si^{2+} and Si^{3+} recoil ion yields. We could detect no C^{3+} ions at all, and the C^{2+} yield was very small. The yield of multicharged scattered ions increases with Z_1, and is largest for Ne^+ projectiles. The scattered ion yield correlates with the number of projectile $2p$ electrons, which increases from one electron in C^+ to five in Ne^+. The $4f\sigma$ orbit is known to be important in electron promotion in many medium mass atomic collisions [30]. This orbital rises rapidly in energy, and crosses many other orbitals in the correlation diagram, so that electrons in this orbital can be promoted to higher shells, or be emitted. However, in contrast to recoil ions, the distance of closest approach at threshold energy, associated with the interaction distance r_0 for production of these scattered ions, is found to increase with Z_1. If $4f\sigma$ orbit promotion were the main source of projectile ionization then the interaction distances would be much larger than observed, and would decrease with increasing Z_1. The multicharged scattered ions must therefore be mainly from some other interaction process than simple $4f\sigma$ electron promotion.

In previous measurements with N^+ and O^+ beams the values of r_0 were found to be similar for recoil and scattered ions, and it was suggested that electron promotion at the same $3d\sigma$ - $3p\pi$ molecular orbital crossing might result in either scattered or recoil multicharged ions. To produce further projectile ionization after electron promotion into the $3p\pi$ state the Auger deexcitation which fills the $3d\sigma$ orbit must occur before the molecule separates into atoms. The present data show that the similarity in r_0 values does not extend to lighter or heavier projectiles. For example, Ne^{2+} and Ne^{3+} ions are produced in Ne^+-Si collisions where the ion-atom trajectories never reach the $3d\sigma$ - $3p\pi$ crossing. It is quite clear that in these collisions the scattered and recoil multicharged ions must be produced by different processes, and it is likely that this is also true in N^+ and O^+, for which these different processes happen to have similar interaction distances.

A two-electron transfer process has been found to be important in determining the final states following ion-gas single collisions. The two electrons make equal and opposite energy transitions in the same collision, so that though there is no crossing in the correlation diagram for single electron state energies, the transition occurs at a near degeneracy in the correlation diagram for the total electron energy. Energy loss spectroscopy measurements in ion–rare-gas collisions by Barat and co-workers [31,32] have identified in C^+-Ne and N^+-Ne the two-electron transitions ($4f\sigma \rightarrow 3d\pi, 3d\sigma \rightarrow 3d\pi$) as important in determining the final charge exchange channels. The interaction distances at which the two-electron transitions take place depend on the relative spacings of the levels, which vary from one element to another. Applying the two-electron transfer process to the present data, the $3s\sigma$ and $3d\pi$ levels change order between C^+ and Ne^+, so that if there is preferential ionization in the lower of the two states, then we would expect silicon ionization in C^+-Si collisions to change to neon ionization in Ne^+-Si collisions, as observed. A difference between our data with the heavier silicon target and the ion–Ne-gas data is that the $3d\sigma$ orbit is much lower in energy, so that the condition for equal and opposite energy transitions may be better satisfied at our observed distances of closest approach if the two electrons are transferred to the $3p\sigma$ orbital. The double-electron-transfer transitions ($4f\sigma \rightarrow 3s\sigma, 3d\sigma \rightarrow 3s\sigma$) and ($4f\sigma \rightarrow 3d\pi, 3d\sigma \rightarrow 3d\pi$) followed by Auger transitions to fill the $3d\sigma$ orbit may produce the multicharged scattered ions. ($4f\sigma \rightarrow 3d\pi, 3d\sigma \rightarrow 3d\pi$) double-electron-transfer transitions may also be responsible for some of the silicon multicharged ion production.

IV. DISCUSSION

These results can be compared with other information which is available on the Z_1 dependence of L-shell vacancy production. X-ray data show large oscillations in the target L-shell x-ray yields, both for solid targets [14] and for gases [13]. These oscillations reach their maximum value where there is a match between the target and projectile shell energies. The maxima are somewhat mismatched when the projectile x rays in solid targets are measured, but the shift in position of the maximum

is consistent with the level energy changes due to the projectile being in an excited or ionized state from previous collisions in the solid. Another characteristic of the x-ray data is that the x rays from the lower Z atom are found to dominate on either side of the $Z_1 = Z_2$ maximum yield, so that target x rays dominate where $Z_1 > Z_2$, and projectile x rays dominate where $Z_1 < Z_2$.

The present data seem to fit the shell matching interpretation of the x-ray data. They would straddle a minimum of the oscillations in the x-ray yield curve as functions of Z_1. Thus the Ne^+-Si data are on the lower Z_1 side of the maximum yield where the shells match at $Z_1 = Z_2$. Multiple ionization of the projectile Ne dominates, in agreement with the model. We could not extend measurements using the present technique into the region of maximum yield nearer to $Z_1 = Z_2$ because of difficulties in kinematically identifying the scattered ions from the recoil ions.

In C^+-Si, the high yield of multiply charged recoiling target ions may be due to this projectile-target combination being on the high Z_1 side of another maximum, where the K-shell energy of the projectile matches the L-shell energy of the silicon target atoms. The shell energies suggest that the maximum x-ray yield and therefore also the maximum multicharged ion production would be expected with a beryllium beam.

The singly charged ion yields are shown in Fig. 5. They have a similar Z_1 behavior to the multicharged ions, with mainly target recoil ions in C^+-Si and projectile ions in Ne^+-Si, suggesting that most of the singly charged ions are produced by the same process as the multicharged ions. This is consistent with scattering processes in which there is "loss of memory" of the incident beam charge state, and very little potential scattering during which the singly charged incident ion preserves its initial charge. If the singly charged ions are the result of Auger transitions which fill L-shell vacancies, as are the multicharged ions, then it is rather surprising that we find no energy thresholds for the singly charged ions down to our lowest beam energies. The collision processes which produce these ions must therefore occur at a very large or an in-

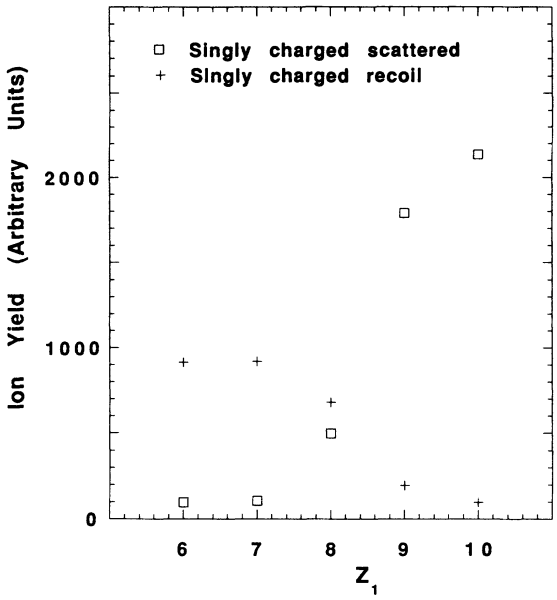

FIG. 5. Yield of singly charged ions. Crosses are for Si^+ recoil ions, and open squares are for scattered ions. There is some uncertainty in comparing the yields from different ion beams because of difficulties in normalization of the beam intensities. This difficulty is not present when comparing the yields of different emitted ions from the same incident ion beam.

distinct interaction radius. Boers [33] reported memory effects in low-energy Ne^+-Cu scattering, where he found different Ne^+ to Ne ratios of scattered particles depending on the charge state of the incident beam. These differences decreased with increasing beam energy and were small at the energies used in Fig. 2. It may be possible to reconcile the lack of energy thresholds with the shell matching Z_1 dependence of the singly charged ion yields by assuming that there is a change in the interaction process, from mainly Auger deexcitation at energies of 10 keV and above, to mainly potential scattering at lower collision energies.

[1] W. F. van der Weg and D. J. Bierman, Physica **44**, 177 (1969).
[2] B. Hird, R. A. Armstrong, and P. Gauthier, Phys. Rev. B **48**, 3654 (1993); Surf. Sci. **292**, 305 (1993).
[3] J.-F. Hennequin, P. Joyes, and R. Casting, Acad. Sci., Ser. B **265**, 315 (1967).
[4] K. Wittmaack, Nucl. Instrum. Methods **170**, 565 (1980).
[5] R. A. Baragiola, L. Nair, and T. E. Madey, Nucl. Instrum. Methods B **58**, 322 (1991).
[6] O. Grizzi and R. A. Baragiola, Phys. Rev. A **35**, 135 (1987).
[7] A. Oliva, A. Bonanno, M. Camarco, and F. Xu, Nucl. Instrum. Methods B **58**, 333 (1991).
[8] M. H. Shapiro and J. Fine, Nucl. Instrum. Methods B **44**, 43 (1989).
[9] S. Valeri, Surf. Sci. Rep. **17**, 85 (1993).
[10] H. D. Betz and L. Grodzins, Phys. Rev. Lett. **25**, 211 (1970).
[11] M. Barat and W. Lichten, Phys. Rev. A **6**, 211 (1972).
[12] J. D. Garcia, R. J. Fortner, and T. M. Kavanagh, Rev. Mod. Phys. **45**, 111 (1973).
[13] F. W. Saris and D. J. Bierman, Phys. Lett. **35A**, 199 (1971).
[14] T. M. Kavanagh, M. E. Cunningham, R. C. Der, R. J. Fortner, J. M. Khan, and E. J. Zaharis, Phys. Rev. Lett. **25**, 1473 (1970).
[15] W. N. Lennard and D. Phillips, Phys. Rev. Lett. **45**, 176 (1980).
[16] W. N. Lennard, T. E. Jackman, and D. Phillips, Phys. Rev. A **24**, 2809 (1981).
[17] J. R. Pierce, *Theory and Design of Electron Beams*, 2nd ed. (Van Nostrand, Princeton, 1954), Chap. IX.

[18] C. C. Hsu, H. Bu, A. Bousetta, J. W. Rabalais, and P. Norlander, Phys. Rev. Lett. **69**, 188 (1992); C. C. Hsu, A. Bousetta, J. W. Rabalais, and P. Norlander, Phys. Rev. B **47**, 2369 (1993).
[19] J. S. Williams, M. C. Ridgway, R. G. Elliman, J. A. Davies, S. T. Johnson, and G. R. Palmer, Nucl. Instrum. Methods B **55**, 602 (1991).
[20] R. E. Schlier and H. E. Farnsworth, J. Chem. Phys. **30**, 917 (1959).
[21] G. Verbist, J. T. Devreese, and H. H. Brongersma, Surf. Sci. **233**, 323 (1990).
[22] D. J. O'Connor and J. P. Biersack, Nucl. Instrum. Methods B **15**, 14 (1986).
[23] J. F. Ziegler, J. P. Biersack, and V. Littmark, in *The Stopping and Range of Ions in Solids*, edited by J. F. Ziegler (Pergamon, New York, 1985).
[24] H. Bu, M. Shi, and R. W. Rabalais, Nucl. Instrum. Methods B **61**, 337 (1991).
[25] F. P. Larkins, J. Phys. B **5**, 571 (1972).
[26] B. Fastrup, G. Hermann, and K. J. Smith, Phys. Rev. A **3**, 1591 (1971).
[27] U. Fano and W. Lichten, Phys. Rev. Lett. **14**, 627 (1965).
[28] J. P. Desclaux, At. Data Nucl. Data Tables **12**, 311 (1973).
[29] F. P. Larkins, J. Phys. B **4**, 1 (1971).
[30] D. Schneider, G. Nolte, U. Wille, and N. Stolterfoht, Phys. Rev. A **28**, 161 (1983).
[31] D. Dowek, J. Krutein, U. Thielmann, J. Fayeton, and M. Barat, J. Phys. B **12**, 2553 (1979).
[32] U. Thielmann, J. Krutein, and M. Barat, J. Phys. B **13**, 4217 (1980).
[33] A. L. Boers, Nucl. Instrum. Methods B **4**, 98 (1984).